Cell autonomous polarization by the planar cell polarity signaling pathway

Alexis T Weiner, Bomsoo Cho, Kaye Suyama, Jeffrey D Axelrod*

Department of Pathology, Stanford University School of Medicine, Stanford, CA 94305, USA

*corresponding author

Abstract

Planar Cell Polarity (PCP) signaling polarizes epithelial cells in a plane orthogonal to their apical-basal axis. A core PCP signaling module both generates molecular asymmetry within cells and coordinates the direction of polarization between neighboring cells. Two subcomplexes of core proteins segregate to opposite sides of the cell, defining a polarity axis. Homodimers of the atypical cadherin Flamingo are thought to be the scaffold upon which these subcomplexes assemble and are required for intercellular polarity signaling. The central role for Flamingo homodimers in scaffolding and intercellular communication suggests that cells in which intercellular signaling via Flamingo is disabled should fail to polarize. We show that cells lacking Flamingo, or bearing a truncated Flamingo that cannot homodimerize do in fact polarize. Cell polarization requires both positive and negative feedback, and in a multicellular tissue, feedback might involve both intracellular and intercellular pathways. We identify positive and negative feedback pathways that operate cell autonomously to drive polarization.

Introduction

The planar cell polarity (PCP) signaling pathway polarizes individual cells and coordinates polarity between cells along an axis parallel to the tissue plane, thereby producing uniform polarity that can span entire tissues[1]. The mechanism by which it polarizes cells has been intensively studied in *Drosophila*. A large body of evidence shows that this mechanism is conserved from flies to humans[2]. Medically important developmental defects and physiological processes in vertebrates are also under control of PCP signaling, motivating considerable interest in understanding the underlying mechanisms of PCP signaling[1,3]. Major advances in understanding molecular mechanisms underlying PCP signaling have come from leveraging of genetic approaches only possible in *Drosophila*, and the evident conservation of mechanism reinforces the utility of flies as a model system.

The core PCP module acts both to generate molecular asymmetry within cells and to coordinate the direction of polarization between neighboring cells. Proteins in this module, including the serpentine protein Frizzled (Fz)[4,5], the seven-pass atypical cadherin Flamingo (Fmi; a.k.a. Starry night)[6,7], the 4-pass protein Van Gogh (Vang; a.k.a. Strabismus)[8,9], and the cytosolic/peripheral membrane proteins Dishevelled (Dsh)[10,11], Diego (Dgo)[12], and the PET/Lim domain protein Prickle (Pk)[13] (reviewed in ref.[1]) segregate within cells to form distinct complexes on opposite sides of the cell. The Dgo-Dsh-Fz-Fmi subcomplex and the oppositely localized Fmi-Vang-Pk subcomplex communicate their presence to the adjacent cell via intercellular bridges formed by

Fmi-Fmi homodimers that signal polarity between cells[14-18]. Any of a number of proposed subtle biasing signals can determine the direction of polarization, and bistability in the core system along with coordination between cells is proposed to reinforce the response[19]. It is thought that both the localized Dgo-Dsh-Fz-Fmi subcomplex and the oppositely localized Fmi-Vang-Pk subcomplex direct cytoskeletal regulators to control morphological outcomes. In the wing, distal Dgo-Dsh-Fz-Fmi and proximal Fmi-Vang-Pk determine the position and orientation of emerging trichomes (a.k.a. prehairs)[20,21].

In single cells that polarize, theory suggests that symmetry breaking requires both positive and negative feedback loops[22,23], and experimental evidence from shmoo formation in budding yeast, chemotaxis of neutrophils and *Dictyostelium*, T cell activation, and developmental cell migration supports this view[24-26]. In these systems, positive feedback acts to localize and reinforce the accumulation and activation of signaling molecules that mark a pole of the cell, while negative feedback excludes or suppresses the accumulation and activation of those factors away from the location of the dominant site. In neutrophils and *Dictyostelium*, two such interlocking systems localize to opposite poles and reinforce each other.

In PCP, both positive and negative feedback are also expected to underlie symmetry breaking and polarization[21,22](Fig 1A-B). It is a logical hypothesis that positive feedback might be a consequence of the cooperative assembly of PCP complexes into clusters. The presence of negative feedback is supported by indirect evidence deriving from mosaic analyses (refs. [14,27] and unpublished). Because PCP is intrinsically multicellular, possibilities for positive and negative feedback are possible that are not available to isolated polarizing cells. Therefore, it is not known whether the ability of PCP to polarize cells independent of intercellular communication is conserved, nor are the operative feedback pathways understood.

Here, we demonstrate that in the *Drosophila* wing, cells deprived of their ability to communicate polarity information from cell to cell can nonetheless polarize. Furthermore, we provide evidence for one positive feedback loop and one negative feedback mechanism and show that they each function in the absence of intercellular polarity communication.

Results

A tool to eliminate intercellular PCP signal transmission

Because Fmi-mediated intercellular PCP communication is a central feature of core PCP function[14-18], it is not apparent that cells stripped of their ability to communicate polarity information through Fmi would remain able to polarize. To address this question, we developed a genetic tool that confers the ability to ‘isolate’ individual cells from their neighbors with respect to PCP information (here referred to as being ‘offline’). Fmi homodimers are essential for communication between proximal and distal (with respect to the wing) complexes on neighboring cells[14-18]. To block intercellular PCP communication, we remove Fmi entirely using *fmi* null alleles, or replace endogenous Fmi with a construct that disrupts *trans* homodimerization but still allows intracellular complexes to assemble (FmiΔcad; lacking all cadherin repeats). Meanwhile, to preserve viability[28], we rescue CNS Fmi expression using the pan-neural GAL4-1407 converted to the Q system, a binary expression system orthogonal to the standard GAL4 system[29]. We verified the absence of Fmi in the wing by antibody staining, and as anticipated, adult offline wings show a strong polarity phenotype similar to that of other core PCP mutants (Supplemental Fig. 1A-B). Note that previously published efforts aiming to employ tissue wide removal of Fmi instead used hypomorphic alleles that did not create a truly null condition.

Offline cells polarize

To determine whether individual offline cells polarize, we generated mosaic expression of Vang::YFP in the offline background, enabling us to unambiguously determine the distribution of Vang within an individual cell. Remarkably, individual cells showed clear asymmetric segregation of Vang::YPF, albeit the signal was weak (Fig. 1C). Furthermore, the direction of cellular polarization was not coordinated across the tissue. We also observed pre-hairs emerging from the side of the cell opposite to Vang::YFP localization, as occurs in wildtype, suggesting that the core PCP system was functioning and that the Fz-Dsh-Dgo complex likely segregates opposite to the Vang-Pk complex (Fig. 1C'-C").

In the *fmi* null wing, the localization of Vang::YFP was weak, but on the other hand, its ability to segregate asymmetrically at all in the absence of Fmi was unexpected. We therefore asked if supplying a truncated Fmi that might template assembly of core PCP complexes[14,17,18,30], but which lacks the ability to communicate between cells, would strengthen the polarized localization of Vang. To do so, we created FmiΔcad, which lacks all cadherin repeats and should therefore fail to trans-homodimerize, but should retain the ability to interact with other core components to facilitate PCP complex assembly. As expected, expression of FmiΔcad under control of the *armadillo* promoter in offline wings failed to correct the strong polarity defect observed in offline wings alone (Supp Fig. 1C). Mosaic expression of Vang::YFP in pupal wings of this genotype produced stronger localization of Vang::YFP compared to offline wings, indicating that templating of PCP complexes indeed enhances polarization (Fig. 1D). We conclude that communication of polarity information between cells is not required for cells to polarize, though their direction of polarization fails to respect the tissue axes. Furthermore, though cells can polarize in the complete absence of Fmi, polarization is more robust when complex assembly is facilitated by a truncated Fmi molecule that lacks all the cadherin repeats but has intact transmembrane and intracellular domains.

It has long been apparent that mutations that disrupt core PCP signaling do not produce randomized polarity of the wing hair pattern despite eliminating detectable asymmetry of core protein localization. Rather, characteristic regions of whorls and more uniform polarity are seen in core PCP mutants. The determinants of this pattern are not well understood, but evidence points to mechanical factors and is described in the Discussion. The wing hair pattern of offline wings strongly resembles that of other core mutants (Supp Fig. 1B), though in this case the orientation of Vang::GFP asymmetric localization correlates to the orientation of hairs. In regions of offline wings where polarity is relatively uniform, so too is the direction of Vang::GFP polarization. In contrast, in regions where the hair polarity is most chaotic, for example near the crossveins, asymmetry of Vang::GFP is very difficult to ascertain (Fig. 1E). From these observations, we infer that the direction of offline cell polarization is likely determined by the same cues that determine the mutant hair polarity pattern.

Positive feedback

Positive feedback via recruitment and activation is a key molecular mechanism used by single cells to drive polarization. For example, yeast positively reinforce polarization by cooperative Cdc42 recruitment and activation, which results in the reduction of lateral diffusion of activated Cdc42-GTP along the membrane and a focused spot of signaling[24]. Similarly, migrating neutrophils exhibit positive feedback of Rac activation, mediated by PIP_3 and Cdc42, producing a leading protrusive edge[25]. In these systems, clustering of key signaling proteins is a critical driver of positive feedback.

Notably, in biochemical analyses of Wnt signaling, Dvl2 (vertebrate Dsh) recruitment by Fz depends on a positive feedback loop involving $PI(4,5)P_2$[31]; the potential existence of a similar mechanism in PCP signaling has not been evaluated. We hypothesized that positive feedback might occur by mutually reinforcing recruitment, clustering and/or stabilization between Fz and Dsh. It is known that during PCP signaling, Fz is required to recruit Dsh to the plasma membrane[32,33], and overexpression of Pk causes excess recruitment of Dsh, Fz and Fmi, also consistent with positive feedback[34]. We therefore wished to test for the possibility of positive feedback between Fz and Dsh by determining whether Fz recruitment, stabilization or clustering might depend on Dsh.

Feedback embedded in the core PCP mechanism[21,35,36] has made it extremely difficult to link an intervention to the immediate downstream consequence (Fig. 1A). To explore more direct relationships between PCP protein localization and effects on other PCP components, we developed a novel genetic 'Velcro' approach to enforce a local asymmetry within the core PCP complex even when PCP signaling is otherwise disrupted.

Our 'Velcro' approach uses N-Cadherin fused to the transmembrane and intracellular domains of Fz (N-Cad::V5-Fz), or to an anti-myc scFv, termed N-Cad::HA-3DX[37], which recruits any myc-tagged protein to cell-cell junctions (Fig. 2A-B). Creating mosaic animals in which N-Cad::V5-Fz or N-Cad::HA-3DX is expressed in clonal cell populations in the pupal wing recruits N-Cad::V5-Fz or Dsh-myc only to cell-cell boundaries where the neighboring cell also expresses the N-Cad construct, thereby enforcing asymmetry in cells at the periphery of the clone (Fig. 2C-D). It is important to note that the N-Cad::V5-Fz is the only Fz in the tissue, such that the background is unpolarized. In contrast, Dsh-myc is uniformly expressed and supports normal polarization when not perturbed by N-Cad::HA-3DX clones. As might be expected, hair polarity is reoriented by both Velcroed Fz and Velcroed Dsh (Supp Fig. 2A-D).

This method allows us to assay recruitment of Fz by Dsh, and *vice versa*, as expected if positive feedback is occurring. We first Velcroed Fz and assayed for Dsh recruitment. To monitor Dsh, we used an antibody that does not readily detect endogenous levels of Dsh. However, N-Cad::V5-Fz is strongly expressed under UAS control, and where N-Cad::V5-Fz localizes, we observe recruitment of endogenous Dsh (Fig. 2E-E'). When N-Cad::V5-Fz is simultaneously monitored via its appended V5 tag, appreciable co-localization of N-Cad::V5-Fz and Dsh are observed in puncta (Fig. 2E"). We then did the reciprocal experiment, Velcroing Dsh-myc and monitoring Fz. As for the Dsh antibody, the Fz antibody does not detect endogenous levels of Fz, but Fz can reliably, though only weakly, be detected where Dsh-myc is localized (Fig. 2F-F"). The Dsh Velcro system is weaker than that of N-Cad::V5-Fz in part because Dsh-myc is expressed at low levels, and in part because endogenous Myc competes with Dsh-myc for binding to N-Cad::HA-3DX (Supp Fig. 2E-E'), accounting for the relatively weak Fz signal. These results clearly demonstrate that not only does Fz recruit Dsh, but Dsh recruits Fz, and the co-localized proteins tend to aggregate in puncta, fulfilling a key prediction for positive feedback.

Negative feedback

In addition to assaying recruitment reflecting positive feedback, the Velcro assay allows us to assay a potential mechanism for negative feedback: exclusion of the Vang/Pk complex from the locations where N-Cad::V5-Fz or Dsh-myc is localized ("inside" boundaries Fig. 3A). For these assays, we chose N-Cad::V5-Fz Velcro because it polarizes more efficiently than N-Cad::HA-3DX Dsh-myc Velcro. We assayed Pk rather than Vang due to the availability of a much more effective antibody. Three possible outcomes were envisioned: *i)* no exclusion, in which case Pk remains uniformly around the cell (black arrow; Fig. 3B); *ii)* exclusion results in only cytoplasmic signal (negative feedback; green arrow); and *iii)* exclusion from Velcro occupied boundaries and

‘capture’ at unoccupied boundaries (yellow arrow).

Indeed, in cells where Fz localization is enforced at all cell edges, very little Pk is observed at the plasma membrane (Fig. 3C-C”) ; red arrowhead), and cytoplasmic Pk is elevated compared to cells outside the clone. In cells where Fz localization is forced to only some cell edges (i.e. at the clone periphery), Pk is not only excluded from N-Cad::V5-Fz occupied edges, but localizes selectively to outside cell edges where N-Cad::V5-Fz is not localized (Fig. 3C ; black arrowhead). Because Pk from the cell outside the clone is also likely to accumulate at that cell interface, A contribution due to exclusion from the clone cell will be apparent as a level higher than at external cell junctions. We therefore quantified and compared intensities at these boundaries and observed that this is the case (Fig. 3F). These observations indicate that negative feedback occurs where Fz is localized.

Feedback in offline cells

Because we observed that offline cells polarize (Fig. 1C), we wished to determine whether the signs of positive and negative feedback just described might also occur in offline conditions. We again employed the N-Cad::V5-Fz Velcro system, this time in offline wings. In the absence of Fmi, N-Cad::V5-Fz is still able to recruit Dsh, though less efficiently than in the presence of Fmi (Fig. 2G-G”). In the presence of Fmi∆cad, Dsh was recruited nearly as efficiently as in the presence of intact Fmi (Fig. 2H-H”). Therefore, consistent with the inference that positive feedback must occur in offline cells, we see one facet of positive feedback in the recruitment of Dsh by Fz.

Similarly, exclusion of Pk by N-Cad::V5-Fz occurs in offline cells. In the absence of Fmi, and in the presence of Fmi∆cad, little or no Pk remains at cell boundaries occupied by N-Cad::V5-Fz (Fig. 3D-F). Exclusion therefore occurs independent of cell-cell PCP communication. Of note, without Fmi, the excluded Pk is not appreciably captured at the unoccupied outside boundaries, while presence of Fmi∆cad facilitates its capture (Fig. 3D’ ; black arrowhead). We conclude from these experiments that negative feedback embodied in the exclusion of Pk by Fz occurs in the absence of cell-cell PCP communication.

Discussion

Fmi homodimers bridging between cells are thought to be the scaffold upon which core PCP complexes are assembled[14,17,18,30]. The central role for Fmi homodimers in scaffolding PCP complexes and in communicating PCP information between cells might suggest that the positive and negative feedback leading to polarization is inextricably linked to intercellular communication[14-18]. Yet, we show here that individual cells polarize in the absence of Fmi. We therefore conclude that individual cells possess machinery that allows them to polarize cell autonomously. The logic of the PCP system thus more closely resembles that of single cell polarizing mechanisms in yeast, neutrophils, *Dictyostelium*, T cells and *C. elegans* embryos[24-26,38] than might otherwise have been expected.

We provide evidence for both positive and negative feedback in core PCP polarization, and show that the two pathways we identify can operate in ‘offline’ cells. Our data suggest positive feedback in the mutual dependence between Fz and Dsh for recruitment to the plasma membrane, likely to clusters, or puncta, and it is in puncta that polarity appears to be generated[27,39,40]. A more formal demonstration of positive feedback will require a demonstration that this mutual dependence leads to an amplification[41]. Our data also demonstrate negative feedback in the exclusion of the proximal complex component Pk from domains where the distal

domain component Fz is enforced. Importantly, neither of these mechanisms require intercellular transmission of PCP information. While in principle, these feedback loops might be sufficient to polarize cells, we do not mean to imply that they are exclusive of other feedback loops. Indeed, we believe it is likely that exclusion of Fz and Dsh by Vang and Pk also occurs[14,27], and it is also possible that positive feedback promotes assembly of the Vang-Pk complex. (Refer to arrows in schematic in Fig 1) Furthermore, additional feedback pathways involving intercellular communication are very likely to operate. We suggest that redundancy in feedback pathways is a likely contributor to the reliable function of PCP polarization.

Because Fmi was thought to template the assembly of PCP signaling complexes[14,17,18,30], the ability of cells to polarize in the absence of Fmi was unexpected. This implies that the other core proteins retain some ability to interact independently of Fmi. Many physical interactions between core proteins have been documented by co-immunoprecipitation that are consistent with this possibility. Fmi likely provides a helpful, albeit non-essential, scaffolding function, as polarization is more robust in the presence of the truncated Fmi∆cad than in its absence. These data imply two separable roles for Fmi, one in templating assembly of complexes within individual cells, and the other in communicating the presence of Dgo-Dsh-Fz or Vang-Pk to the adjacent cell.

As noted above, strong mutations of core polarity components, with the exception of *pk*, produce very similar whorl patterns of adult wing hairs, and this observation now extends to the *fmi*^{null} (offline) condition. While the determinants of this pattern are not well understood, experiments that modify the mechanical environment by eliminating wing veins substantially simplify the hair polarity pattern of PCP mutants[42]. Because vein cells have smaller apical surfaces than other cells, the cell packing patterns are necessarily less regular near veins, and additional evidence has shown that cell packing contributes to polarization and *vice versa*[43,44]. Thus, the core mutant wing hair polarity pattern may derive from the cell packing pattern. Additional mechanical influences across the developing wing, such as cell flow have also been proposed[45]. In vertebrate systems, tissue deformation via tension has also been shown to orient PCP patterns[46-48]. In one case, this was shown to depend on microtubules[48]. In the fly wing, since microtubules both contribute and respond to cell shape[49], and apical microtubules are proposed to provide directional bias to core PCP polarization[50], we hypothesize that they have a role in this process. Notably, despite cells polarizing their core proteins in offline cells, this fails to correct the aberrant hair polarity pattern. We propose this is due to their inability to align their polarities via Fmi interactions.

We show here that the PCP system retains the ability to polarize cells cell autonomously when stripped of its ability to transmit polarity information between neighboring cells. One positive and one negative feedback mechanism are identified that could support this polarization. Future studies will be required to further characterize these feedback mechanisms and to define other intracellular and intercellular mechanisms that are likely to also contribute to polarization.

Materials and Methods

Drosophila Husbandry and Genetics

Flies stocks were raised on standard fly food at 25ºC. Heat shock protocols were performed on third instar larvae at 37ºC and moved back to 25ºC until selection of pupae. Standard

Drosophila genetic techniques were used to create recombinant chromosomes. Compound balanced fly stocks were then generated to create stable fly lines.

Homology assisted CRISPR knock-in (HACK) was used as described in Lin and Potter[29] to convert 1407-GAL4 to QF2-1407.

Drosophila genotypes

Genotypes of experiments by figure are listed below.

Figure 1:

yw hsFLP ; QF2-1407, *fmi*^{E59} / *fmi*^{E45} ; QUAS-fmi (F17) / TM2, act>>vang-YFP

yw hsFLP ; QF2-1407, *fmi*^{E59} / arm-*fmiΔcad*, *fmi*^{E45} ; QUAS-fmi (F17) / TM2, act>>vang-YFP

Figure 2:

dsh^{V26}, dsh-V5-6xmyc ; hsFLP ; act>>GAL4 / UAS-Ncad::HA-3DX

hsFLP ; UAS-N-Cad::V5-Fz / act>>GAL4

hsFLP ; UAS-N-Cad::V5-Fz, *fz*^{R52} / act>>GAL4, *fz*^{R52}

Figure 3:

hsFLP ; UAS-Ncad::V5-Fz, *fz*^{R52} / act>>GAL4, *fz*^{R52}

yw hsFLP ; QF2-1407, *fmi*^{E59} / *fmi*^{E45} ;
QUAS-fmi (F17), *fz*^{R52} / act>>GAL4, UAS-N-Cad::V5-Fz, *fz*^{R52}

yw hsFLP ; QF2-1407, *fmi*^{E59} / arm-*fmiΔ*cad, *fmi*^{E45} ; QUAS-fmi (F17), *fz*^{R52} / act>>GAL4, UAS-Ncad-V5-fz, *fz*^{R52}

Supplemental Figure 1:

QF2-1407, *fmi*^{E59} / *fmi*^{E45} ; QUAS-fmi (F17)

QF2-1407, *fmi*^{E59} / arm-*fmiΔcad*, *fmi*^{E45} ; QUAS-fmi (F17)

Supplemental Figure 2:

hsFLP ; UAS-N-Cad::V5-Fz, *fz*^{R52} / act>>GAL4, *fz*^{R52}

hsFLP ; *dsh*^{V26}, dsh-myc ; act>>GAL4, UAS-RFP / UAS-Ncad::HA-3DX

Cloning and novel *Drosophila* strain construction

pQUAST-fmi

Full length *fmi* cDNA from UAS-fmi (ref [7]) was subcloned in two EcoR1-Xho1fragments into pQUAST (#24349; Addgene) and transformed into w^{1118} flies to generate random genomic insertions.

pUAST-N-Cadherin::HA-3DX
A fragment of N-Cadherin cDNA (gift of Tom Clandinin) from the first aa to the SacII site, removing the C-terminus including the β-catenin binding site, was subcloned into pUAST. After mutating the internal SacII site, the HA-3DX sequence was generated by PCR from (ref [37]) and appended to the SacII site in N-Cadherin. The resulting plasmid was transformed into w^{1118} flies to generate random genomic insertions.

pUAST-N-cad::V5-Fz
The first 2915aa extracellular domain of N-Cadherin was generated by PCR from pUAST-N-Cadherin::HA-3DX using the following two primers:
Forward:
AAGAGAACTCTGAATAGGGAATTGGGAATTCATGGCGGCACGACGTTGC
Reverse:
CCGCCAGAGCCTGTGCCGCTATCACGGGATGGCGTCAATACAC
The resulting fragment contained the extracellular portion of Ncadherin (2915aa) with the described linker and a V5 epitope tag.
The Fz transmembrane and C-terminus (final 347aa) was generated by PCR from (ref. [51]) using the following primers:
Forward:
ATCCCGTGATAGCGGCACAGGCTCTGGCGGCAAACCGATTCCGAACCCGCTGCTGGGCCTGGATAGCACCAGCGGAGGCGGTGGCATGTTCTTCCCGGAGAGAGAAAG
Reverse:
CTTCACAAAGATCCTCTAGACTACACGTACGCCTGCGCCCG
The N-Cadherin and Fz fragments were cloned into EcoR1 and Xba1 digested pUAST.
The resulting plasmid was transformed into w^{1118} flies to generate random genomic insertions.

pCas4-dsh-V5-6myc
The V5-6myc fragment, flanked by Xba1 sites was generated by touch down PCR using pUAST-Rab35-6myc (Addgene #53503) as template.
Forward primer:
TCTAGAAGCGGCACAGGCTCTGGCGGCAAACCGATTCCGAACCCGCTGCTGGGCCTGGATAGCACCAGTGGTGGATCCACCATGGAGCAAAAGCTC
Reverse primer:
TCTAGAATACCGGTGATTACAAGTCCTCTTC
pCas4-dsh from ref.[32] was digested with Xba1 and the V5-6xmyc fragment appended. The resulting plasmid was transformed into w^{1118} flies to generate random genomic insertions and an X chromosome insertion was recombined onto a dsh^{v26} f^{36a} chromosome.

Pupal wing dissections and immunohistochemistry

Immunohistochemistry of pupal wings was performed using the following protocol. White prepupae were selected, raised at 25°C and aged (indicated by figure with apf) to desired time point. Pupae were then dissected from their pupal casing, affixed to double sided tape on a slide and were directly whole animal fixed for 30 min in 4% paraformaldehyde at room temperature. Pupal wings were then dissected from fixed pupae and moved to PBST (PBS with 0.1% Triton X-100). Primary antibody incubations (1:200 dilution) were performed overnight at 4°C and then washed in PBST for a total of 15 minutes. Incubations with secondary antibodies (and phalloidin

if noted) were then performed for an hour at room temperature in PBST. Wings were then washed in PBST for a total of 15 minutes. Stained wings were mounted using 12 µl Vectashield mounting medium (Vector Laboratories). Primary antibodies were as follows: mouse monoclonal anti-V5 (1:200 dilution, Thermo-fisher, R960-25), guinea pig polyclonal anti-Pk[C] (1:800 dilution, ([32]), mouse monoclonal anti-Fmi (1:200 dilution, DSHB), rat monoclonal anti::HA (clone 3F10, 1:200 dilution, Roche), rat monoclonal anti-dEcad (1:200 dilution, DSHB), rabbit polyclonal anti-dsh (1:200)[52], mouse monoclonal anti-fz (1:200 DSHB 1C11), and mouse monoclonal anti myc (Thermo-fischer 1:200 sc-40). Secondary antibodies from Thermo Fisher Scientific were as follows: 488-donkey anti-mouse, 488-goat anti-rabbit, 596-donkey anti-mouse, 633-goat anti-guinea pig, Alexa 350 conjugated phalloidin was obtained from Thermo Fisher Scientific.

Confocal microscopy and quantification

Immunostained pupal wing images were taken with a Leica TCS SP8 AOBS confocal microscope and processed in Fiji (imagej). Quantification of relative fluorescence intensity of pk staining as shown in Figure 3, was performed by tracing approximately 40µm along 8-10 cell membranes of either clone boundary or at a distance away from the clone. Adult wings were dissected and washed with 70% EtOH and mounted in DPX (Sigma) solution. All adult wings were imaged on a Nikon Eclipse E1000M equipped with a Spot Flex camera (Model15.2 64 MP).

All wing images are shown with proximal to the left and anterior to the top.

Acknowledgements

We would like to thank members of the Axelrod lab for fruitful discussions. Stocks obtained from the Bloomington Drosophila Stock Center (NIH P40OD018537) were used in this study.

This work was funded by NIH R35GM131914 (J.D.A.). The funders had no role in study design, data collection and analysis, decision to publish, or preparation of the manuscript.

Conflict of interest

The authors declare that the research was conducted in the absence of any commercial or financial relationships that could be construed as a potential conflict of interest.

References

1 Butler, M. T. & Wallingford, J. B. Planar cell polarity in development and disease. *Nature reviews. Molecular cell biology* **18**, 375-388 (2017). https://doi.org:10.1038/nrm.2017.11

2 Hale, R. & Strutt, D. Conservation of Planar Polarity Pathway Function Across the Animal Kingdom. *Annu Rev Genet* **49**, 529-551 (2015). https://doi.org:10.1146/annurev-genet-112414-055224

3 Simons, M. & Mlodzik, M. Planar Cell Polarity Signaling: From Fly Development to Human Disease. *Annu Rev Genet* **42**, 517-540 (2008).

4 Vinson, C. R. & Adler, P. N. Directional non-cell autonomy and the transmission of polarity information by the *frizzled* gene of *Drosophila*. *Nature* **329**, 549-551 (1987).

5 Vinson, C. R., Conover, S. & Adler, P. N. A *Drosophila* tissue polarity locus encodes a protein containing seven potential transmembrane domains. *Nature* **338**, 263-264 (1989).
6 Chae, J. *et al.* The Drosophila tissue polarity gene starry night encodes a member of the protocadherin family. *Development* **126**, 5421-5429 (1999).
7 Usui, T. *et al.* Flamingo, a seven-pass transmembrane cadherin, regulates planar cell polarity under the control of Frizzled. *Cell* **98**, 585-595 (1999).
8 Taylor, J., Abramova, N., Charlton, J. & Adler, P. N. Van Gogh: a new Drosophila tissue polarity gene. *Genetics* **150**, 199-210 (1998).
9 Wolff, T. & Rubin, G. M. Strabismus, a novel gene that regulates tissue polarity and cell fate decisions in Drosophila. *Development* **125**, 1149-1159 (1998).
10 Klingensmith, J., Nusse, R. & Perrimon, N. The *Drosophila* segment polarity gene dishevelled encodes a novel protein required for response to the wingless signal. *Genes and Development* **8**, 118-130 (1994).
11 Thiesen, H., Purcell, J., Bennett, M., Kansagara, D., Syed, A. & Marsh, J. L. *dishevelled* is required during *wingless* signaling to establish both cell polarity and cell identity. *Development* **120**, 347-360 (1994).
12 Feiguin, F., Hannus, M., Mlodzik, M. & Eaton, S. The ankyrin repeat protein Diego mediates Frizzled-dependent planar polarization. *Dev Cell* **1**, 93-101. (2001).
13 Gubb, D. *et al.* The balance between isoforms of the prickle LIM domain protein is critical for planar polarity in Drosophila imaginal discs. *Genes Dev* **13**, 2315-2327 (1999).
14 Chen, W. S. *et al.* Asymmetric homotypic interactions of the atypical cadherin flamingo mediate intercellular polarity signaling. *Cell* **133**, 1093-1105 (2008).
15 Struhl, G., Casal, J. & Lawrence, P. A. Dissecting the molecular bridges that mediate the function of Frizzled in planar cell polarity. *Development* **139**, 3665-3674 (2012). https://doi.org:10.1242/dev.083550
16 Lawrence, P. A., Casal, J. & Struhl, G. Cell interactions and planar polarity in the abdominal epidermis of Drosophila. *Development* **131**, 4651-4664 (2004).
17 Strutt, D. & Strutt, H. Differential activities of the core planar polarity proteins during Drosophila wing patterning. *Dev Biol* **302**, 181-194 (2007).
18 Strutt, H. & Strutt, D. Differential stability of flamingo protein complexes underlies the establishment of planar polarity. *Curr Biol* **18**, 1555-1564 (2008). https://doi.org:10.1016/j.cub.2008.08.063
19 Axelrod, J. D. & Tomlin, C. J. Modeling the control of planar cell polarity. *Wiley Interdiscip Rev Syst Biol Med* **3**, 588-605 (2011). https://doi.org:10.1002/wsbm.138
20 Adler, P. N. & Wallingford, J. B. From Planar Cell Polarity to Ciliogenesis and Back: The Curious Tale of the PPE and CPLANE proteins. *Trends Cell Biol* **27**, 379-390 (2017). https://doi.org:10.1016/j.tcb.2016.12.001
21 Axelrod, J. D. in *Encyclopedia of Cell Biology* Vol. 3 (ed Ralph A. Bradshaw and Philip D. Stahl) 199-207 (Academic Press, 2016).
22 Meinhardt, H. Computational modelling of epithelial patterning. *Curr Opin Genet Dev* **17**, 272-280 (2007). https://doi.org:10.1016/j.gde.2007.05.004
23 Gierer, A. & Meinhardt, H. A theory of biological pattern formation. *Kybernetik* **12**, 30-39 (1972). https://doi.org:10.1007/BF00289234
24 Chiou, J. G., Balasubramanian, M. K. & Lew, D. J. Cell Polarity in Yeast. *Annu Rev Cell Dev Biol* **33**, 77-101 (2017). https://doi.org:10.1146/annurev-cellbio-100616-060856
25 Van Keymeulen, A. *et al.* To stabilize neutrophil polarity, PIP3 and Cdc42 augment RhoA activity at the back as well as signals at the front. *J Cell Biol* **174**, 437-445 (2006). https://doi.org:10.1083/jcb.200604113
26 Meili, R. & Firtel, R. A. Two poles and a compass. *Cell* **114**, 153-156 (2003). https://doi.org:10.1016/s0092-8674(03)00553-1

27 Cho, B., Pierre-Louis, G., Sagner, A., Eaton, S. & Axelrod, J. D. Clustering and negative feedback by endocytosis in planar cell polarity signaling is modulated by ubiquitinylation of prickle. *PLoS Genet* **11**, e1005259 (2015). https://doi.org:10.1371/journal.pgen.1005259
28 Matsubara, D., Horiuchi, S. Y., Shimono, K., Usui, T. & Uemura, T. The seven-pass transmembrane cadherin Flamingo controls dendritic self-avoidance via its binding to a LIM domain protein, Espinas, in Drosophila sensory neurons. *Genes Dev* **25**, 1982-1996 (2011). https://doi.org:10.1101/gad.16531611
29 Lin, C. C. & Potter, C. J. Editing Transgenic DNA Components by Inducible Gene Replacement in Drosophila melanogaster. *Genetics* **203**, 1613-1628 (2016). https://doi.org:10.1534/genetics.116.191783
30 Bastock, R., Strutt, H. & Strutt, D. Strabismus is asymmetrically localised and binds to Prickle and Dishevelled during Drosophila planar polarity patterning. *Development* **130**, 3007-3014 (2003).
31 Mahoney, J. P., Bruguera, E. S., Vasishtha, M., Killingsworth, L. B., Kyaw, S. & Weis, W. I. PI(4,5)P2-stimulated positive feedback drives the recruitment of Dishevelled to Frizzled in Wnt-beta-catenin signaling. *Sci Signal* **15**, eabo2820 (2022). https://doi.org:10.1126/scisignal.abo2820
32 Axelrod, J. D. Unipolar membrane association of Dishevelled mediates Frizzled planar cell polarity signaling. *Genes Dev* **15**, 1182-1187. (2001).
33 Wu, J., Jenny, A., Mirkovic, I. & Mlodzik, M. Frizzled-Dishevelled signaling specificity outcome can be modulated by Diego in Drosophila. *Mech Dev* **125**, 30-42 (2008). https://doi.org:S0925-4773(07)00187-6 [pii] 10.1016/j.mod.2007.10.006
34 Tree, D. R., Shulman, J. M., Rousset, R., Scott, M. P., Gubb, D. & Axelrod, J. D. Prickle mediates feedback amplification to generate asymmetric planar cell polarity signaling. *Cell* **109**, 371-381 (2002). https://doi.org:10.1016/S0092-8674(02)00715-8
35 Amonlirdviman, K., Khare, N. A., Tree, D. R., Chen, W. S., Axelrod, J. D. & Tomlin, C. J. Mathematical modeling of planar cell polarity to understand domineering nonautonomy. *Science* **307**, 423-426 (2005).
36 Le Garrec, J. F., Lopez, P. & Kerszberg, M. Establishment and maintenance of planar epithelial cell polarity by asymmetric cadherin bridges: a computer model. *Dev Dyn* **235**, 235-246 (2006).
37 Fujiwara, K., Poikonen, K., Aleman, L., Valtavaara, M., Saksela, K. & Mayer, B. J. A single-chain antibody/epitope system for functional analysis of protein-protein interactions. *Biochemistry* **41**, 12729-12738 (2002). https://doi.org:bi0263309 [pii]
38 Lang, C. F. & Munro, E. The PAR proteins: from molecular circuits to dynamic self-stabilizing cell polarity. *Development* **144**, 3405-3416 (2017). https://doi.org:10.1242/dev.139063
39 Strutt, H., Warrington, S. J. & Strutt, D. Dynamics of core planar polarity protein turnover and stable assembly into discrete membrane subdomains. *Dev Cell* **20**, 511-525 (2011). https://doi.org:10.1016/j.devcel.2011.03.018
40 Strutt, H., Gamage, J. & Strutt, D. Robust Asymmetric Localization of Planar Polarity Proteins Is Associated with Organization into Signalosome-like Domains of Variable Stoichiometry. *Cell reports* **17**, 2660-2671 (2016). https://doi.org:10.1016/j.celrep.2016.11.021
41 Mitrophanov, A. Y. & Groisman, E. A. Positive feedback in cellular control systems. *Bioessays* **30**, 542-555 (2008). https://doi.org:10.1002/bies.20769
42 Hogan, J., Valentine, M., Cox, C., Doyle, K. & Collier, S. Two frizzled planar cell polarity signals in the Drosophila wing are differentially organized by the Fat/Dachsous pathway. *PLoS Genet* **7**, e1001305 (2011). https://doi.org:10.1371/journal.pgen.1001305

43 Ma, D., Amonlirdviman, K., Raffard, R. L., Abate, A., Tomlin, C. J. & Axelrod, J. D. Cell packing influences planar cell polarity signaling. *Proc Natl Acad Sci U S A* **105**, 18800-18805 (2008). https://doi.org:0808868105 [pii] 10.1073/pnas.0808868105
44 Classen, A.-K., Anderson, K. I., Marois, E. & Eaton, S. Hexagonal packing of Drosophila wing epithelial cells by the planar cell polarity pathway. *Dev Cell* **9**, 805-817 (2005).
45 Aigouy, B. *et al.* Cell flow reorients the axis of planar polarity in the wing epithelium of Drosophila. *Cell* **142**, 773-786 (2010). https://doi.org:10.1016/j.cell.2010.07.042
46 Aw, W. Y., Heck, B. W., Joyce, B. & Devenport, D. Transient Tissue-Scale Deformation Coordinates Alignment of Planar Cell Polarity Junctions in the Mammalian Skin. *Curr Biol* **26**, 2090-2100 (2016). https://doi.org:10.1016/j.cub.2016.06.030
47 Hirano, S., Mii, Y., Charras, G. & Michiue, T. Alignment of the cell long axis by unidirectional tension acts cooperatively with Wnt signalling to establish planar cell polarity. *Development* **149** (2022). https://doi.org:10.1242/dev.200515
48 Chien, Y. H., Srinivasan, S., Keller, R. & Kintner, C. Mechanical Strain Determines Cilia Length, Motility, and Planar Position in the Left-Right Organizer. *Dev Cell* **45**, 316-330 e314 (2018). https://doi.org:10.1016/j.devcel.2018.04.007
49 Singh, A. *et al.* Polarized microtubule dynamics directs cell mechanics and coordinates forces during epithelial morphogenesis. *Nat Cell Biol* **20**, 1126-1133 (2018). https://doi.org:10.1038/s41556-018-0193-1
50 Galic, M. & Matis, M. Polarized trafficking provides spatial cues for planar cell polarization within a tissue. *Bioessays* **37**, 678-686 (2015). https://doi.org:10.1002/bies.201400196
51 Strutt, D. I. Asymmetric localization of Frizzled and the establishment of cell polarity in the *Drosophila* wing. *Molecular Cell* **7**, 367-375 (2001).
52 Willert, K., Brink, M., Wodarz, A., Varmus, H. & Nusse, R. Casein kinase 2 associates with and phosphorylates dishevelled. *Embo J* **16**, 3089-3096 (1997).

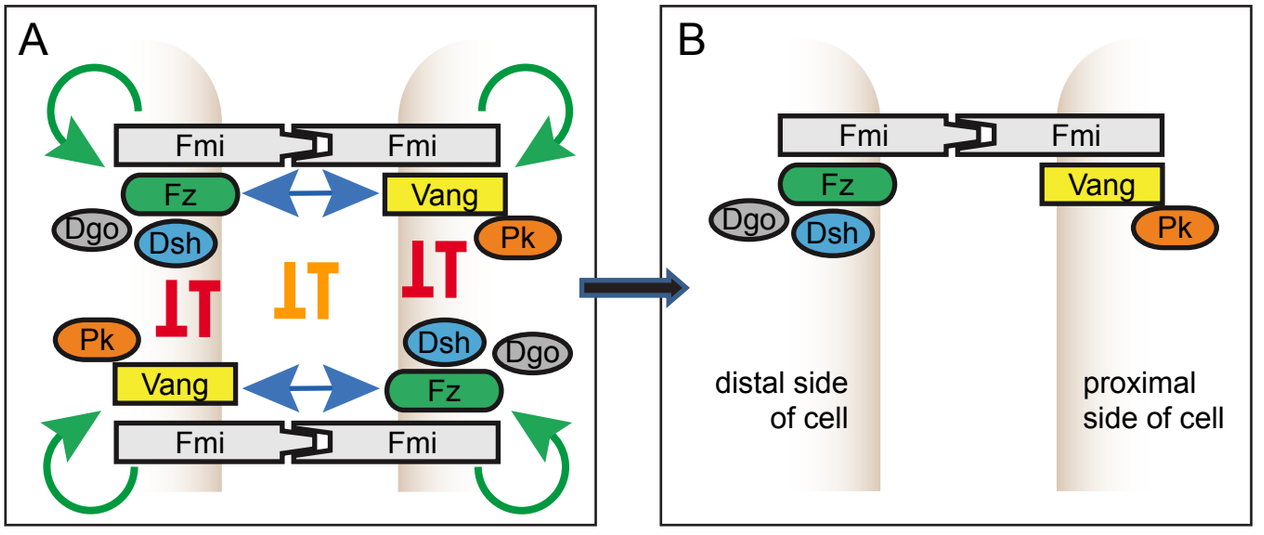
A
Fmi
Fmi
Fz
Vang
Dgo
Dsh
Pk
Pk
Vang
Dsh
Dgo
Fz
Fmi
Fmi
B
Fmi
Fmi
Fz
Vang
Dgo
Dsh
Pk
distal side
of cell
proximal
side of cell

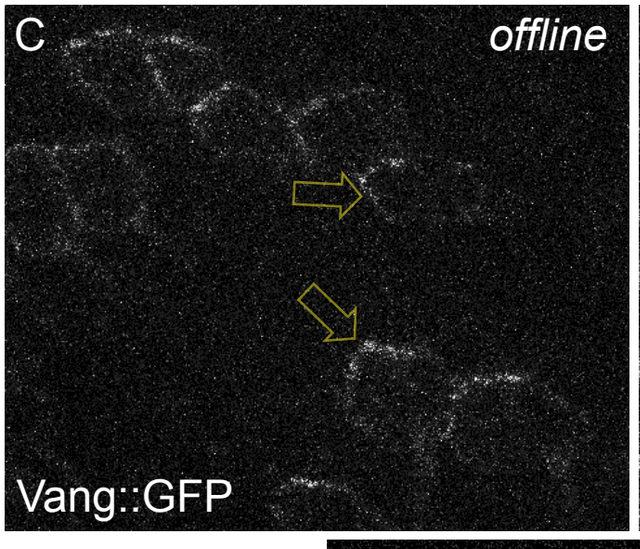
C
offline
Vang::GFP

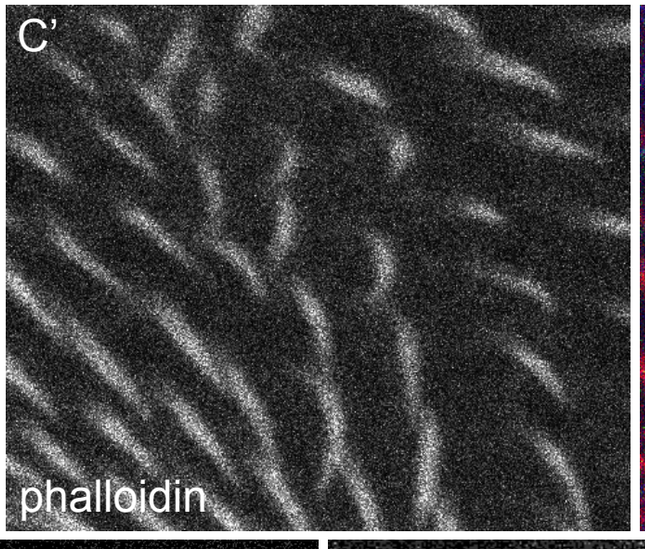
C'
phalloidin

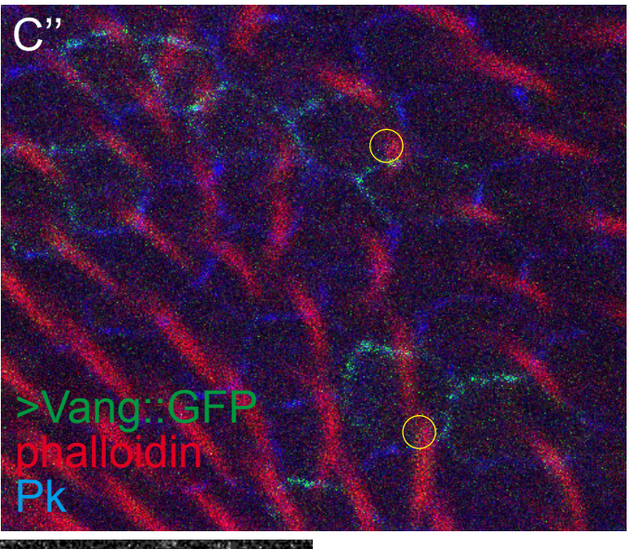
C''
>Vang::GFP
phalloidin
Pk

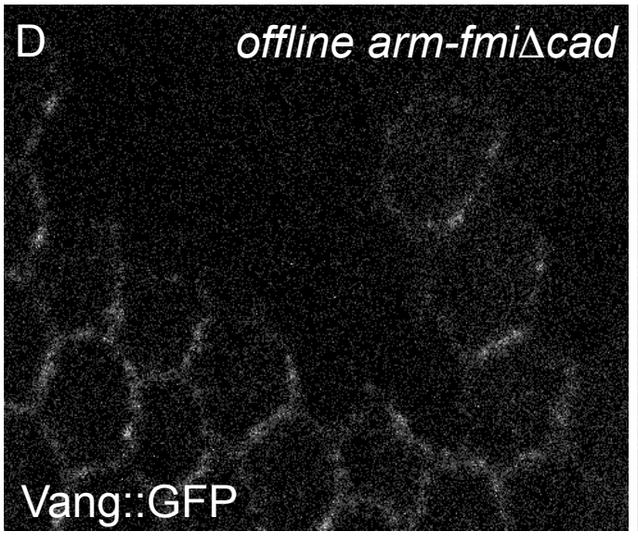
D
offline arm-fmiΔcad
Vang::GFP

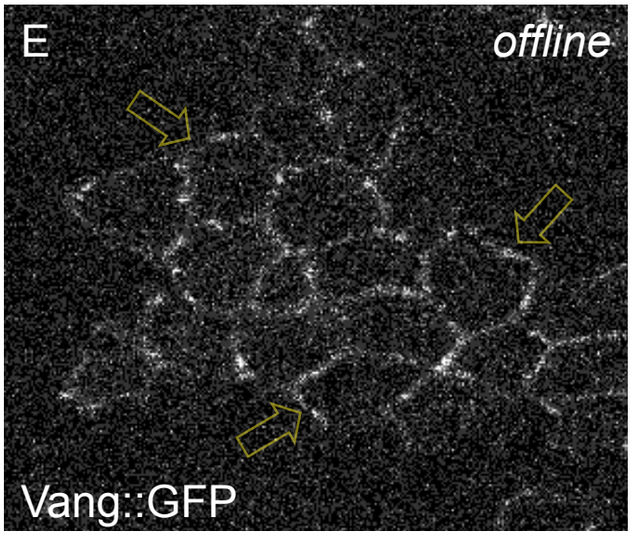
E
offline
Vang::GFP

Figure 1. Offline cells polarize.
A,B. Schematic of PCP complex composition and organization. Asymmetric Fmi bridges linking Fz-Dsh-containing sub-complexes to Vang-Pk-containing sub-complexes (A) sort themselves to yield predominantly one sub-complex on one side of the cell and the other sub-complex on the opposite side of the cell (B). Green and blue arrows represent hypothesized positive feedback pathways and red and orange arrows represent hypothesized negative feedback pathways. Blue and orange pathways require intercellular communication whereas green and red might work cell-autonomously.
C-C''. Vang::GFP clones in offline (*fmi*^{null}) wings reveal asymmetric segregation as occurs in wildtype wings. The direction of polarization deviates from the proximal-distal axis (arrows) and corresponds to the direction of prehairs (C,C'). Prehairs arise on the side of the cell opposite to the Vang::GFP crescents as occurs in wildtype (C'; circles).
D. Vang::GFP clones in an offline+FmiDcad wing.
E. Vang::GFP clone near the anterior crossvein in the region of the swirl. The location corresponds to the yellow box in Supplemental Figure 1B.
Scale bars = 5 μm.

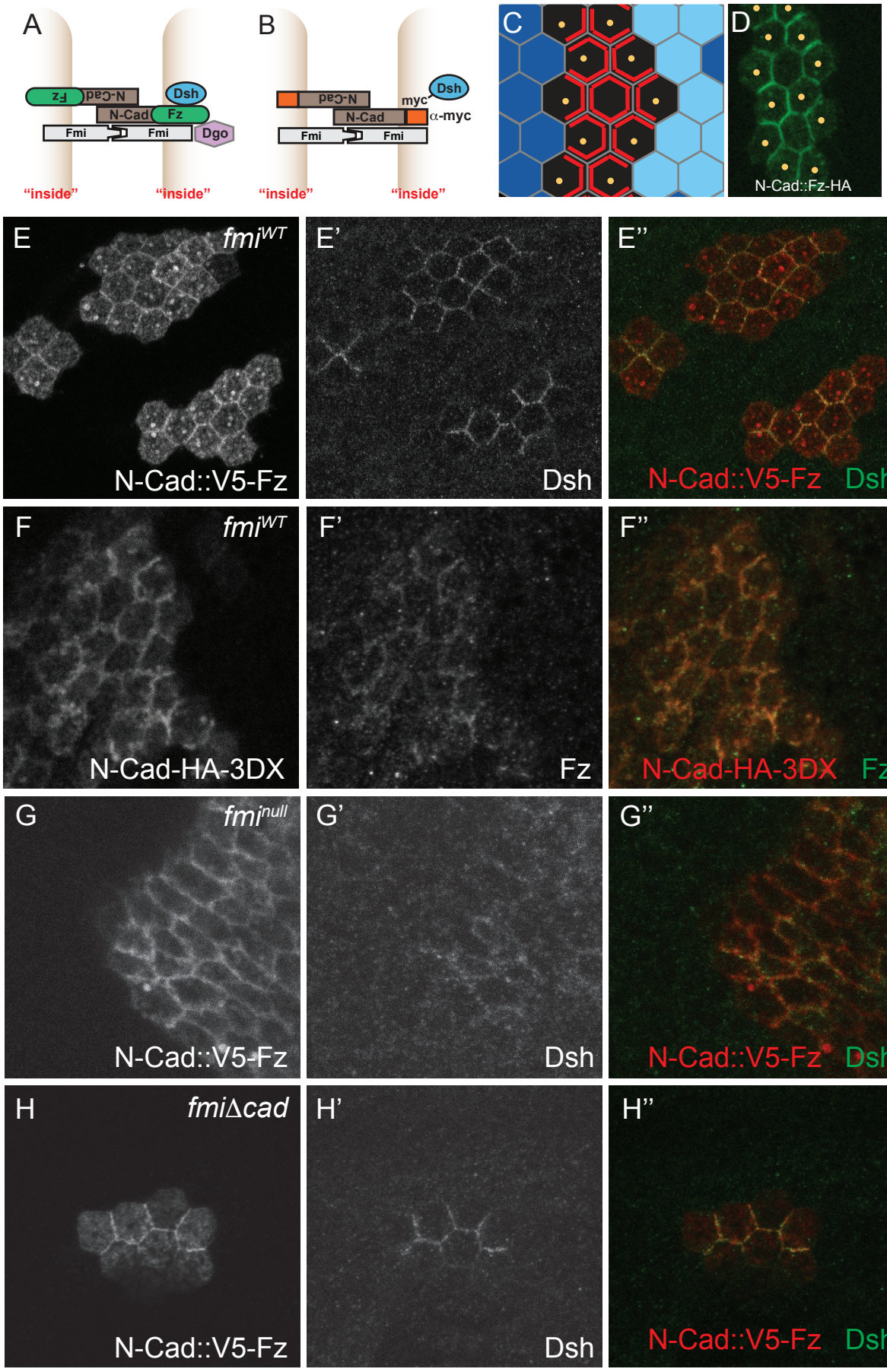
A
Fz
N-Cad
Dsh
N-Cad
Fz
Fmi
Fmi
Dgo
"inside"
"inside"
B
N-Cad
Dsh
myc
N-Cad
α-myc
Fmi
Fmi
"inside"
"inside"
C
D
N-Cad::Fz-HA
E
fmiWT
N-Cad::V5-Fz
E'
Dsh
E''
N-Cad::V5-Fz
Dsh
F
fmiWT
N-Cad-HA-3DX
F'
Fz
F''
N-Cad-HA-3DX
Fz
G
fminull
N-Cad::V5-Fz
G'
Dsh
G''
N-Cad::V5-Fz
Dsh
H
fmiΔcad
N-Cad::V5-Fz
H'
Dsh
H''
N-Cad::V5-Fz
Dsh

Figure 2. Velcroed Fz recruits Dsh and Velcroed Dsh recruits Fz in wildtype and offline backgrounds.

A. Schematic of the Fz Velcro system. Clonal N-Cad::V5-Fz expression recruits N-Cad::V5-Fz selectively to shared cell junctions (C). No endogenous Fz is present.

B. Schematic of the Dsh Velcro system. Clonal expression of N-Cad3DX in wings uniformly expressing Dsh-myc at low levels recruits Dsh-myc to shared cell junctions (C).

C. Schematic of clonal expression (black) recruiing Velcroed components (red) to shared cell junctions. At the periphery of the clone, recruitment is to some but not all cell junctions

D. N-Cad::V5-Fz stained with anti-V5showing localization to shared cell junctions.

E-E''. N-Cad::V5-Fz clones in *fz*^{null} background (Velcroed Fz) stained for V5, Dsh (E') and merged (E''). Note that the Dsh antibody is not sensitive enough to detect endogenous Dsh, so it only detects Dsh colocalizing with N-Cad::V5-Fz where it is recruited to sufficient levels for detection.

F-F''. N-Cad::HA-3DX clone in a Dsh-myc expressing wing (Velcroed Dsh) stained for HA to detect N-Cad::HA-3DX (F), Fz (F') and merged F''. Note that the Fz antibody is not sensitive enough to detect endogenous Fz, so it only detects Fz colocalizing with N-Cad::HA-3DX where it is recruited to sufficient levels for detection.

G-G''. N-Cad::V5-Fz clones in *fz*^{null}, *fmi*^{null} background (Velcroed Fz, offline) stained for V5 (G), Dsh (G') and merged (G'').

H-H''. N-Cad::V5-Fz clones in *fz*^{null}, *fmi*^{null}, *arm-fmi∆cad* background (Velcroed Fz, offline with Fmi∆cad) stained for V5 (H), Dsh (H') and merged (H'').

Scale bars = 5 μm.

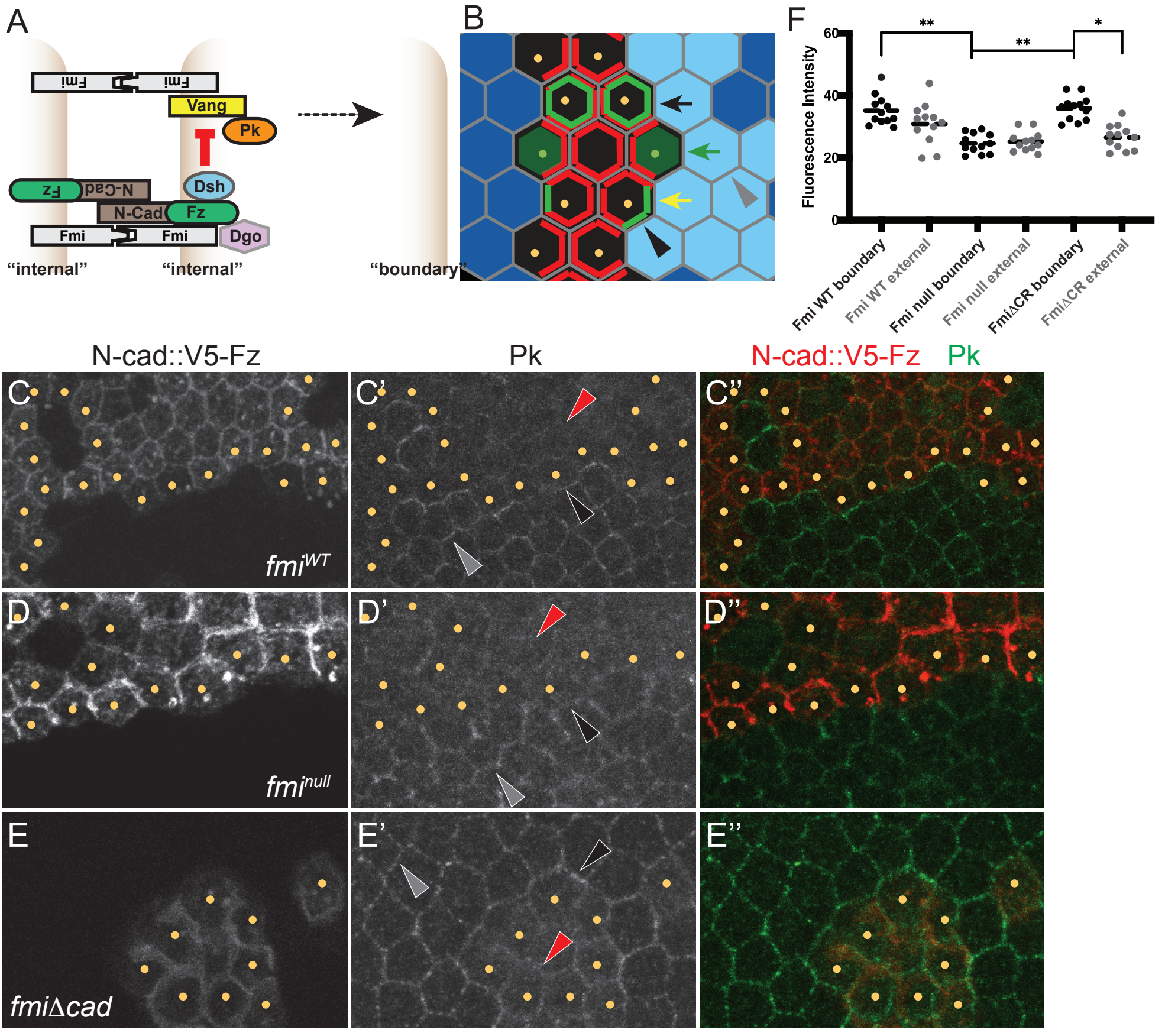
A
Fmi
Fmi
Vang
Pk
Dsh
Fz
N-Cad
N-Cad
Fz
Fmi
Fmi
Dgo
"internal"
"internal"
"boundary"
B
F
Fluorescence Intensity
60
40
20
0
**
**
*
Fmi WT boundary
Fmi WT external
Fmi null boundary
Fmi null external
FmiΔCR boundary
FmiΔCR external
N-cad::V5-Fz
Pk
N-cad::V5-Fz Pk
C
C'
C''
fmiWT
D
D'
D''
fminull
E
E'
E''
fmiΔcad

Figure 3. Velcroed Fz excludes Pk in wildtype and offline backgrounds.
A. Schematic of Velcroed Fz excluding the Vang-Pk subcomplex.
B. Potential outcomes of the exclusion experiment showing localization of Pk: no exclusion (black arrow), exclusion and accumulation in cytoplasm (green arrow), and exclusion and capture of Pk at cell boundaries lacking N-Cad::V5-Fz (clone "boundary"). To quantify Pk capture at clone boundaries, intensity line scans were done at clone boundaries (black arrowhead) and compared to intensity linescans of nearby external cell boundaries (gray arrowhead).
C-C''. N-Cad::V5-Fz clones in *fz*^{null} background (Velcroed Fz) stained for V5 (C), Pk (C') and merge (C''). Pk is excluded from internal clone boundaries where N-Cad::V5-Fz localizes and cytoplasmic level is increased. Pk is captured at clone boundaries (quantified in F).
D-D''. N-Cad::V5-Fz clones in *fz*^{null}, *fmi*^{null} background (Velcroed Fz, offline) stained for V5 (D), Pk (D') and merge (D''). Pk is excluded from internal clone boundaries where N-Cad::V5-Fz localizes and cytoplasmic level is increased. Pk is excluded from internal clone boundaries where N-Cad::V5-Fz localizes and cytoplasmic level is increased. Pk is not captured at clone boundaries (quantified in F).
E-E''. N-Cad::V5-Fz clones in *fz*^{null}, *fmi*^{null}, *arm-fmi∆cad* background (Velcroed Fz, offline with Fmi∆cad) stained for V5 (E), Pk (E') and merge (E''). Pk is excluded from internal clone boundaries where N-Cad::V5-Fz localizes and cytoplasmic level is increased. Pk is excluded from internal clone boundaries where N-Cad::V5-Fz localizes and cytoplasmic level is increased. Pk is captured at clone boundaries (quantified in F).
F. Quantification of cell boundary intensity linescans as described in B for the results in C-E (see Materials and Methods). Significance was tested with a one way ANOVA to compare mean variance. ** denotes $p < .01$ and * denotes $p < .05$.
Scale bars = 5 μm.

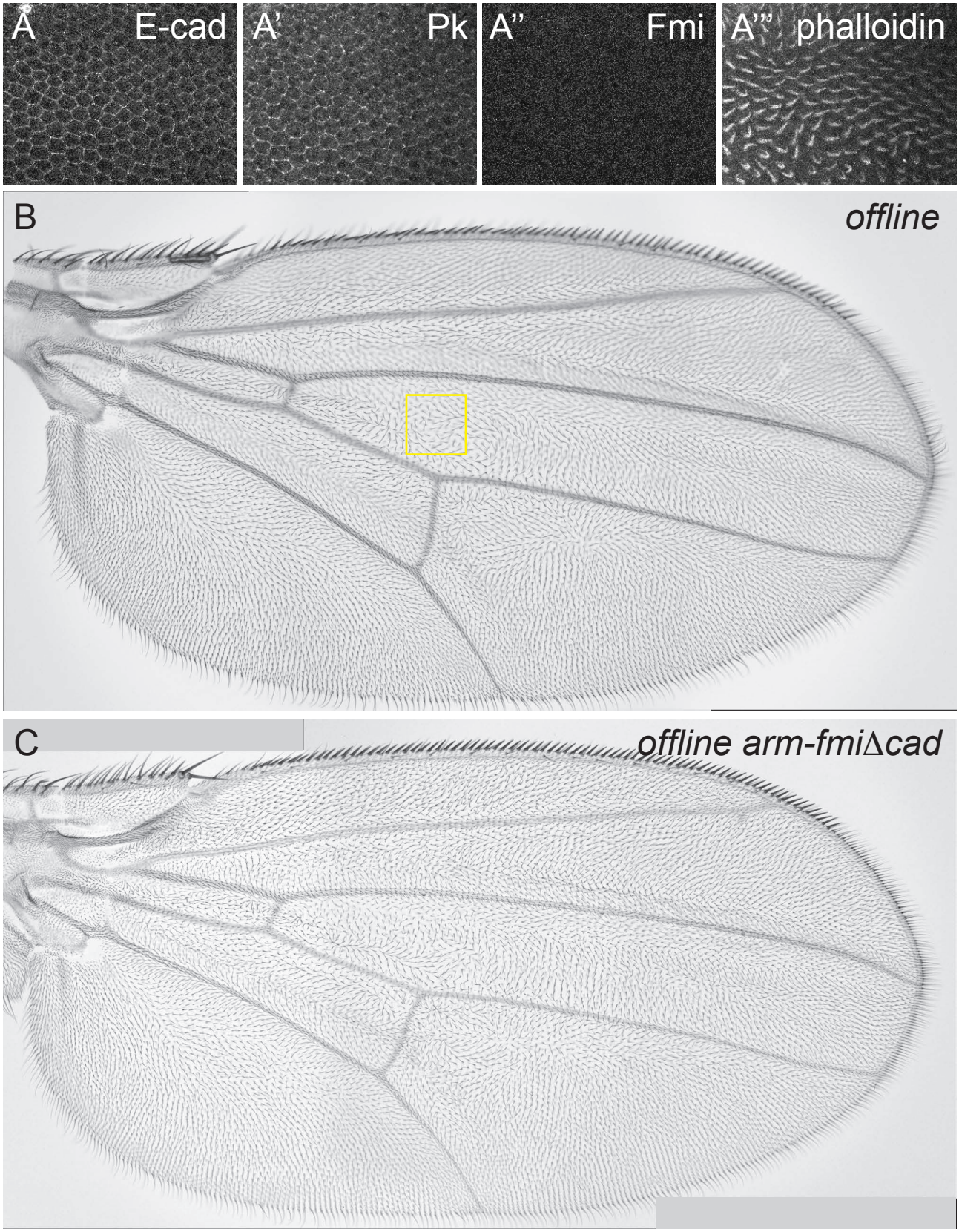
A
E-cad
A'
Pk
A''
Fmi
A'''
phalloidin
B
offline
C
offline arm-fmiΔcad

Supplemental Figure 1. Validation of the offline system.
A-A'''. Region of a *fmi*^{null} offline (QF2-1407, *fmi*^{E59} / *fmi*^{E45} ; QUAS-fmi (F17)) wing stained for E-Cadherin (A), Pk (A'), Fmi (A'') and phalloidin, demonstrating no detectable Fmi. Scale bar = 10 μm.
B. Adult *fmi*^{null} offline wing showing characteristic core PCP mutant phenotype.
C. Adult *fmi*^{null} *arm-fmiΔcad* offline wing showing the same characteristic core PCP mutant phenotype.

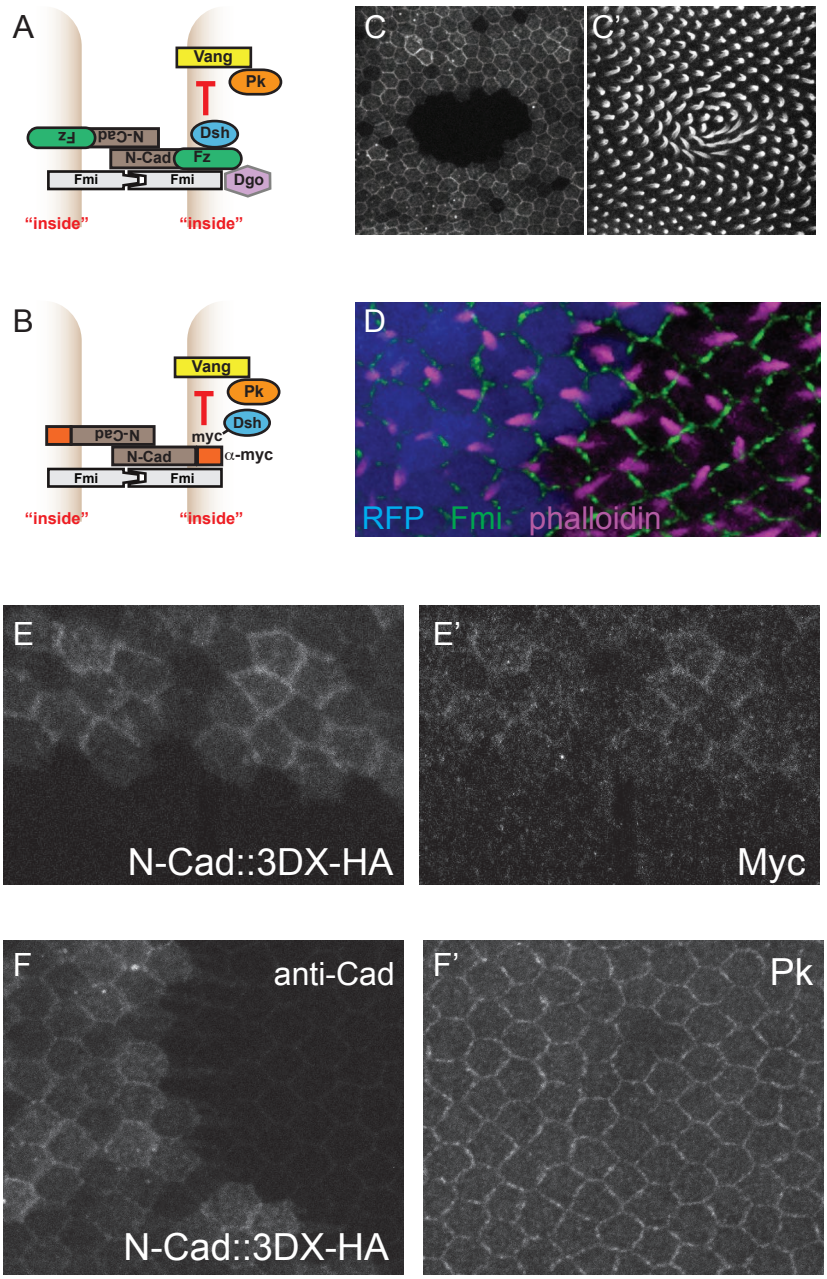
A
Vang
Pk
Dsh
N-Cad
Fz
Fz
N-Cad
Fmi
Fmi
Dgo
"inside"
"inside"
C
C'
B
Vang
Pk
Dsh
N-Cad
myc
N-Cad
α-myc
Fmi
Fmi
"inside"
"inside"
D
RFP
Fmi
phalloidin
E
N-Cad::3DX-HA
E'
Myc
F
anti-Cad
N-Cad::3DX-HA
F'
Pk

Supplemental Figure 2. Validation of the Velcro system.
A. Schematic of the Fz Velcro exclusion assay.
B. Schematic of the Dsh Velcro exclusion assay.
C,C'. A large clone expressing Fz Velcro wrapping around a region lacking Velcro, stained for V5 (N-Cad::V5-Fz; C) and phalloidin (C'). Polarity is perturbed by the clone boundary.
D. Portion of a Dsh Velcro clone marked with RFP (blue), stained for Fmi (green) and phalloidin (magenta), showing prehairs of reversed polarity near the clone boundary. This is an example of a strong phenotype for Dsh Velcro (hsFLP ; dsh^{V26}, dsh-myc ; act>>GAL4, UAS-RFP / UAS-Ncad::HA-3DX). Many clones altered hair polarity only weakly or not at all.
E,E'. N-Cad::HA-3DX expressed without Dsh-myc. Staining for HA (E) and with anti-myc reveals that endogenous Myc is recruited.
F,F'. N-Cad::HA-3DX expressed alone, stained for anti-N-Cadherin (F) and for Pk (F'), demonstrating that N-Cad::HA-3DX itself does not disturb Pk localization. Note that the anti-N-Cadherin antibody detects Cadherin repeats from both N-Cad and endogenous E-Cad that is visible outside the N-Cad expression region.
Scale bars = 5 μm.